Scattering of waves by three-dimensional obstacles in elastic metamaterials with zero index

Fengming Liu,[1,2,*] Feng Zhang,[1,2] Wei Wei,[3] Ni Hu,[1,2] Gang Deng,[1,2] and Ziyu Wang[4,5,†]

[1]*Hubei Collaborative Innovation Center for High-efficiency Utilization of Solar Energy, Hubei University of Technology, Wuhan 430068, China*

[2]*School of Science, Hubei University of Technology, Wuhan 430068, China*

[3]*Hubei Cancer Hospital, Wuhan 430079, China*

[4]*School of Physics and Technology, Wuhan University, Wuhan 430072, China*

[5]*Materials and Technology Institute, Dongfeng Motor, Wuhan 430056, China*

(Received 24 July 2016; revised manuscript received 6 November 2016; published 14 December 2016)

The scattering of elastic waves by three-dimensional obstacles in isotropic elastic zero-index-metamaterials (ZIM) is theoretically investigated. We show that the zero values of each single effective parameter and their various combinations of the elastic ZIM can produce different types of wave propagation. Particularly, there is no mode conversion when either longitudinal (P) wave or transverse (S) wave is scattered by the obstacles in a specific type of double-ZIM (DZIM), possessing near zero reciprocal of shear modulus and near zero mass density. When the obstacle is off resonance, elastic waves are scarcely scattered; nevertheless, the scattering cross section of the obstacle can be drastically enhanced by orders of magnitude when it is on resonance. While in another type of DZIM possessing near zero reciprocal of bulk modulus and near zero mass density, mode conversion occurs during the scattering process and many other transmission characteristics are also different to the former. Moreover, enhanced transmission can be realized for various types of single-ZIM (SZIM) by introducing obstacles, and numerical analysis shows that the enhanced transmission is due to resonant modes arisen in the embedded obstacles. We expect that our findings could have potential practical application, such as seismic protection and on-chip phononic devices.

DOI: 10.1103/PhysRevB.94.224102

I. INTRODUCTION

The scattering of elastic waves by an obstacle is a fundamental physical problem of classical elastodynamics that impacts a wide variety of applications, such as the dynamic stress concentration, nondestructive testing, earth-structure interaction in an earthquake, and calculation of band structure of a phononic crystal [1–8]. It has attracted a great deal of attention from numerous researchers, starting from the pioneering work of Ying and Truell [1]; however, most of the previous publications studied the scattering of elastic waves by various types of obstacles in conventional elastic media. Nowadays, the study of metamaterials has been a very popular research topic across different disciplines due to its many potentially revolutionary applications. Thus, it will be an interesting problem to investigate the scattering of elastic waves by an obstacle, but this time, in the emerging elastic metamaterials [9–13]. A category of metamaterials that has attracted increased attention recently is zero-index-metamaterials (ZIM) whose permittivity and permeability are simultaneously or individually near zero. Their exciting anomalous properties lead to many intriguing phenomena and applications, such as tailoring the wave fronts of radiation field, squeezing of electromagnetic energy at will, manipulating electromagnetic wave propagation through ZIM waveguides by imbedding proper defects, and enhancing optical nonlinearities [14–25]. Meanwhile, the concept of ZIM has been extended to acoustic and elastic media, and several schemes have been proposed to realize them [26–36]. However, because of the complexity of the scattering of elastic waves in solid structure, limited works [37–39] were devoted to elastic ZIM; thus further research is needed.

In general, when a wave of either longitudinal (P) or transverse (S) type is incident on an elastic obstacle, scattered waves of both types are produced, a process known as "mode conversion" [40]. However, here we show that, in a specific type of elastic double-ZIM (DZIM) possessing near zero reciprocal of shear modulus $1/\mu$, near zero mass density ρ and ordinary bulk modulus κ (denoted by type I DZIM), mode conversion does not occur when either P wave or S wave is scattered by the embedded obstacles. As the analog of the ZIMs for electromagnetic waves and for acoustic waves, when the embedded obstacle is off resonance, the type I DZIM can serve as cloak for full elastic waves. However, note that when the embedded obstacle is on resonance, the scattering cross section of the obstacle can be drastically enhanced by orders of magnitude, which results in a total blocking of the incident wave for a very large metamaterials region by using even a single resonant obstacle. A simple analytic model is proposed to capture the physics of this anomalous phenomenon, and then the elastic Mie-like scattering theory is used to verify this analytic model. Another type of DZIM has also been investigated. This type of DZIM has near zero reciprocal of bulk modulus $1/\kappa$, near zero mass density ρ and ordinary shear modulus μ (denoted by type II DZIM). Obviously, the type II DZIM has double near zero parameters only for the P wave, while single near zero parameter for the S wave. We find that unlike the type I DZIM, there is mode conversion when the P wave is scattered by the obstacles embedded in the type II DZIM. However, since the wavelength of the P wave in the type II DZIM also approaches infinity, the scattering is weak and the incident P wave can

*Corresponding author: fmliu@mail.hbut.edu.cn

†Corresponding author: zywang@whu.edu.cn

transmit through the type II DZIM slab with little disturbance and preserve its P wave form, except the situation of the appearance of resonant modes in the obstacles. In addition, to thoroughly understand the propagation characteristic of various kinds of elastic ZIM, we also investigate single-ZIM (SZIM) possessing either near zero reciprocal of bulk/shear modulus or near zero mass density. Analysis shows that only part of the incident wave can transmit through the SZIM slab without embedded obstacles, and the transmission is inversely proportional to the width of the slab. However, if obstacles are embedded into the SZIM slab, the transmission can be strongly enhanced. The local resonant modes arisen in the obstacles account for the enhanced transmission. Since mode conversion does not happen and the wave natures of the P wave and two S waves always remain intact during the scattering process in the type I DZIM, we investigate the possibility of independent control the propagation of the P wave and two S waves by using complicated inclusions (such as a cuboid obstacle). It is shown that, due to the low symmetry of the cuboid obstacle, even the two originally degenerate S waves can be manipulated separately. Finally, we propose a three-dimensional (3D) phononic crystal, which can be mapped to an elastic material with effective zero $1/\mu_{\text{eff}}$ and zero ρ_{eff}; thus, it can be a good candidate to achieve the type I DZIM structure experimentally.

II. NUMERICAL ANALYSIS OF THE SCATTERING CHARACTERISTIC OF ELASTIC WAVES BY 3D OBSTACLES IN THE ELASTIC ZIM

The geometry of the 3D structure under consideration is illustrated in Fig. 1. It consists of four distinct regions: The left and right regions are background mediums (with mass density ρ_0, bulk modulus κ_0, and shear modulus μ_0) and are separated by the elastic ZIM slab with effective mass density ρ_1, bulk modulus κ_1, and shear modulus μ_1. A spherical solid obstacle with radius r_d, mass density ρ_d, bulk modulus κ_d, and shear modulus μ_d is embedded in the ZIM slab. The periodic boundary condition is applied to the four lateral boundaries

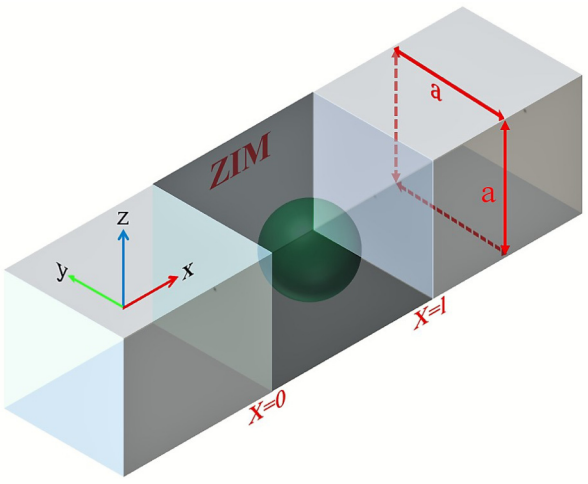

FIG. 1. Schematic of the unit cell of our periodic system along the y and z direction; the unit cell consists of the background medium, the elastic ZIM, and an embedded spherical obstacle.

in the numerical simulation. Note that the utilization of the slab and the periodic boundary condition here is just for the convenience of conducting the numerical simulation. It will be shown below that the structure period a has a different influence on the transmission characteristic of the type I DZIM and type II DZIM slab.

A. Case of the type I DZIM

We first investigate the propagation characteristics of the type I DZIM slab without inclusion. The governing equations for the elastic waves in an isotropic solid can be written as

$$\begin{aligned}
\rho\frac{\partial v_x}{\partial t} &= \frac{\partial \tau_{xx}}{\partial x}+\frac{\partial \tau_{yx}}{\partial y}+\frac{\partial \tau_{zx}}{\partial z},\\
\rho\frac{\partial v_y}{\partial t} &= \frac{\partial \tau_{xy}}{\partial x}+\frac{\partial \tau_{yy}}{\partial y}+\frac{\partial \tau_{zy}}{\partial z},\\
\rho\frac{\partial v_z}{\partial t} &= \frac{\partial \tau_{xz}}{\partial x}+\frac{\partial \tau_{yz}}{\partial y}+\frac{\partial \tau_{zz}}{\partial z},
\end{aligned} \tag{1}$$

$$\begin{aligned}
\frac{\partial \tau_{xx}}{\partial t} &= (\kappa+\mu)\frac{\partial v_x}{\partial x}+(\kappa-\mu)\frac{\partial v_y}{\partial y}+(\kappa-\mu)\frac{\partial v_z}{\partial z},\\
\frac{\partial \tau_{yy}}{\partial t} &= (\kappa-\mu)\frac{\partial v_x}{\partial x}+(\kappa+\mu)\frac{\partial v_y}{\partial y}+(\kappa-\mu)\frac{\partial v_z}{\partial z},\\
\frac{\partial \tau_{zz}}{\partial t} &= (\kappa-\mu)\frac{\partial v_x}{\partial x}+(\kappa-\mu)\frac{\partial v_y}{\partial y}+(\kappa+\mu)\frac{\partial v_z}{\partial z},\\
\frac{\partial \tau_{xy}}{\partial t} &= \mu\left(\frac{\partial v_x}{\partial y}+\frac{\partial v_y}{\partial x}\right),\\
\frac{\partial \tau_{xz}}{\partial t} &= \mu\left(\frac{\partial v_x}{\partial z}+\frac{\partial v_z}{\partial x}\right),\\
\frac{\partial \tau_{yz}}{\partial t} &= \mu\left(\frac{\partial v_y}{\partial z}+\frac{\partial v_z}{\partial y}\right),
\end{aligned} \tag{2}$$

where $v_i(i=x,y,z)$ represents the velocity field, which is the derivative of the displacement field $u_i(i=x,y,z)$ with respect to time, and $\tau_{ij}(i,j=x,y,z)$ represents the stress tensor. Equations (1) and (2) represent Newton's law and the generalized Hook law, respectively. For plane waves in a homogeneous elastic medium propagating along the x direction, Eqs. (1) and (2) can be simplified to

$$\rho\frac{\partial v_y}{\partial t}=\frac{\partial \tau_{xy}}{\partial x},\quad \frac{\partial \tau_{xy}}{\partial t}=\mu\frac{\partial v_y}{\partial x} \tag{3}$$

for the y direction S wave,

$$\rho\frac{\partial v_z}{\partial t}=\frac{\partial \tau_{xz}}{\partial x},\quad \frac{\partial \tau_{xz}}{\partial t}=\mu\frac{\partial v_z}{\partial x} \tag{4}$$

for the z direction S wave and

$$\rho\frac{\partial v_x}{\partial t}=\frac{\partial \tau_{xx}}{\partial x},\quad \frac{\partial \tau_{xx}}{\partial t}=(\kappa+\mu)\frac{\partial v_x}{\partial x} \tag{5}$$

for the P wave, respectively. In the type I DZIM region, as $1/\mu_1$ tends to zero, the velocity fields v_y in Eq. (3) and v_z in Eq. (4) must be constant to keep τ_{xy} and τ_{xz} as a finite value, respectively. Since the displacement field is the integral of the velocity field with respect to time, u_y and u_z are also constant in the type I DZIM region for y direction S wave and z direction S wave incidence, respectively. While for the P

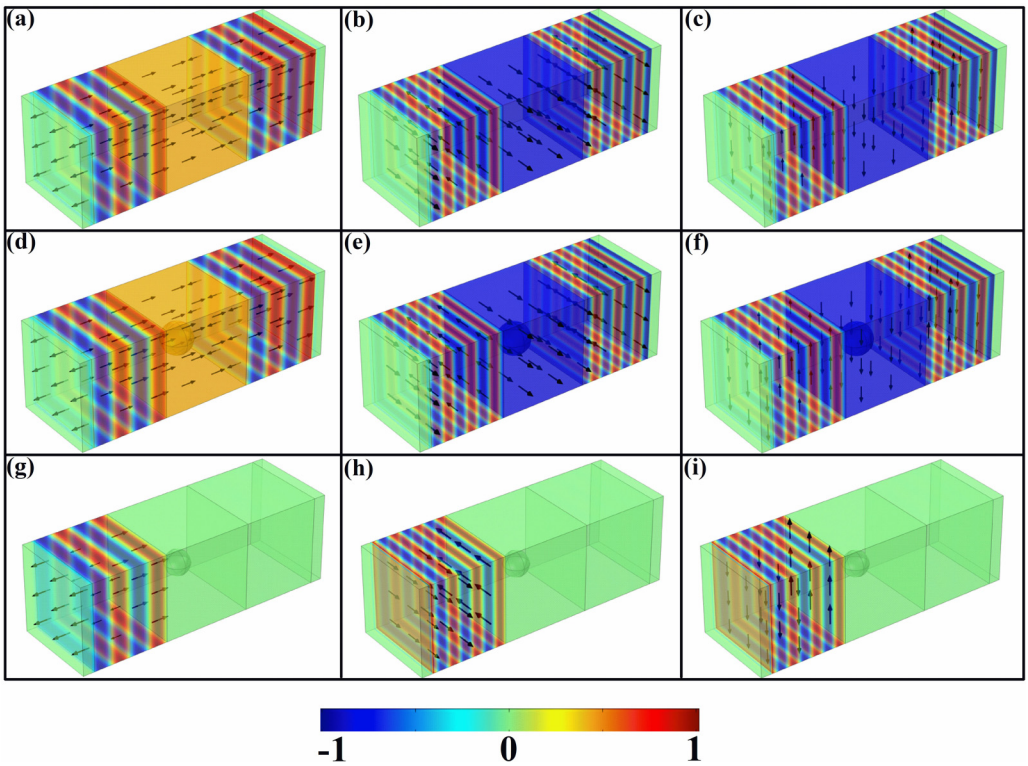

FIG. 2. The numerically simulated displacement field distributions of the incident waves transmitting through the type I DZIM slab without inclusion (a)–(c), with steel inclusions (d)–(f), and the incident waves are totally blocked (g)–(i). The arrows denote the directions of the displacement. Different columns represent the results of incident P wave, y direction S wave, and z direction S wave, respectively. The simulation domain is terminated in the propagation direction with perfectly matched layers (PML), and the periodic boundary condition is applied to the four lateral boundaries in the simulation.

wave incidence, as $1/(\mu_1+\kappa_1)$ tends to zero too, the velocity field v_x (and thus the displacement field u_x) in Eq. (5) must be constant to keep τ_{xx} as a finite value. Numerical simulations are carried out by using the finite element method (FEM) to verify the analysis. In the simulation, the background medium is Si with $\rho_0 = 2.53\times10^3\ \mathrm{kg/m^3}$, $c_{0,l} = 6.72\times10^3\ \mathrm{m/s}$, and $c_{0,t} = 4.13\times10^3\ \mathrm{m/s}$, and we have set $\rho_1 = 0.001\rho_0$, $1/\mu_1 = 0.001(1/\mu_0)$, and $\kappa_1 = \kappa_0$ for the type I DZIM. The frequency of the incident wave is $f_0 = 500$ Hz. Figures 2(a)–2(c) show the displacement field distributions of the P wave, y direction S wave, and z direction S wave transmitting through the type I DZIM slab, respectively. The displacement fields u_{1x}, u_{1y} and u_{1z} in the type I DZIM region are uniform indeed. Next, we consider the problem of introducing solid obstacles into the type I DZIM slab. Figures 2(d)–2(f) show the numerically simulated displacement field distributions of the P wave, y direction S wave, and z direction S wave transmitting through the type I DZIM slab embedded with steel spheres ($r_d = 5.3$ m), respectively. Compared to Figs. 2(a)–2(c), the displacement field distributions outside the spheres are the same. Thus, even though inclusions have been introduced, the displacement fields u_{1x}, u_{1y}, and u_{1z} in the type I DZIM region are still uniform, and there is no scattering and no mode conversion occurring for all three types of incident waves. This phenomenon can be explained by utilizing the constitutive relation of isotropic elastic solid under which condition μ_1 diverges in the type I DZIM region. In general, if there are elastic discontinuities, one needs to consider the complete equation of generalized Hook' law [Eq. (2)] instead of Eqs. (3)–(5). Since v_x, v_y, and v_z all appear in Eq. (2), P wave, y direction S wave, and z direction S wave are coupled. However, in the type I DZIM region, after both sides are divided by μ_1 and under the condition μ_1 diverge, Eq. (2) can be simplified to

$$\begin{aligned} 0 &= \frac{\partial v_x}{\partial x} - \frac{\partial v_y}{\partial y} - \frac{\partial v_z}{\partial z}, \quad 0 = -\frac{\partial v_x}{\partial x} + \frac{\partial v_y}{\partial y} - \frac{\partial v_z}{\partial z}, \\ 0 &= -\frac{\partial v_x}{\partial x} - \frac{\partial v_y}{\partial y} + \frac{\partial v_z}{\partial z}, \quad 0 = \frac{\partial v_x}{\partial y} + \frac{\partial v_y}{\partial x}, \\ 0 &= \frac{\partial v_x}{\partial z} + \frac{\partial v_z}{\partial x}, \quad = \frac{\partial v_y}{\partial z} + \frac{\partial v_z}{\partial y}. \end{aligned} \tag{6}$$

Solutions $v_{1x} = \text{constant}$, $v_{1y} = v_{1z} = 0$ (for purely P wave), $v_{1y} = \text{constant}$, $v_{1x} = v_{1z} = 0$ (for purely y direction S wave) and $v_{1z} = \text{constant}$, and $v_{1x} = v_{1y} = 0$ (for purely z direction S wave) can satisfy Eq. (6). Thus, the purely P wave, the purely y direction S wave, or the purely z direction S wave can still propagate in the type I DZIM region, even though elastic discontinuities have been introduced. However, when the size of the embedded sphere is changed to have the radius $r_d = 4.17$ m, contrary to our expectation, the incident waves are totally blocked by the type I DZIM slab, as shown in Figs. 2(g)–2(i). Such anomalous total blocking is completely counterintuitive, considering the wavelength in the type I DZIM is 10^3 times larger than that in the background medium, and the impedance of the type I DZIM matches with that of

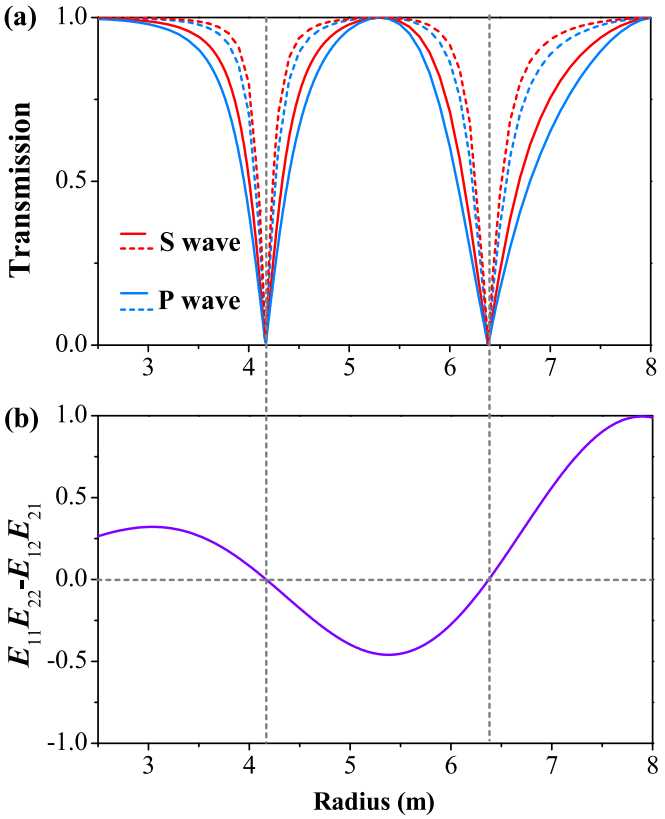

FIG. 3. The numerically calculated transmission coefficients (a) of the type I DZIM slab with spherical obstacles and the values of expression $E_{11}E_{22}-E_{12}E_{21}$ (b) as a function of the radius r_d of the spherical obstacle, respectively. In (a), the solid and dotted lines represent the systems with different structure periods $a = 30$ m and $a = 45$ m, respectively.

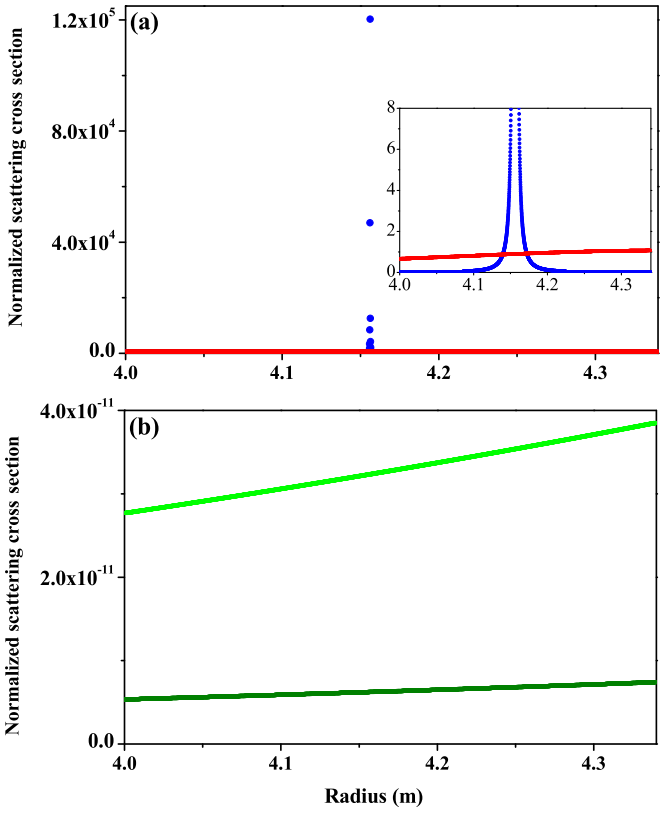

FIG. 4. (a) The $n = 1$ order normalized scattering cross section of a single spherical obstacle in the type I DZIM (blue dotted line) and in the background medium (red solid line) as a function of the radius r_d of the spherical obstacle. Inset shows the zoom-in view. (b) The $n = 0$ (olive line) and $n = 2$ (green line) order normalized scattering cross section of the same spherical obstacle in the type I DZIM as a function of the radius r_d.

the background medium. In the following, a simple analytic model [41] is proposed to capture the essence of the physics. Details of the analytic model can be found in the Appendix. As an example, steel spheres are considered here. Figures 3(a) and 3(b) show the numerically calculated transmission coefficients and the values of expression $E_{11}E_{22} - E_{12}E_{21}$ as a function of the radius r_d of the sphere, respectively. Note that the effective parameters of ZIM are almost zero only when the frequency equals a specific frequency; thus, we have fixed the frequency of the incident wave $f_0 = 500$ Hz, while the radius r_d of the sphere becomes a variable in Figs. 3(a) and 3(b). It can be seen that each time the expression $E_{11}E_{22} - E_{12}E_{21}$ equals zero, the transmission coefficients of both incident S and P waves equal zero indeed. It should be noted that both the P and S waves are controlled by the same factor because of the high symmetry of the spherical obstacle (the resonances induced by the x direction vibration of the P wave and by the y or z directions vibration of the S waves are equivalent).

It can also be seen in Fig. 3(a) that when we increase the structure period $a = 30$ m to $a = 45$ m, total blocking still occurs at the same radius of the sphere. In fact, we can increase the structure period even much larger and still achieve the total blocking at the same radius of the sphere. This anomalous phenomenon can be explained by using the elastic Mie-like scattering theory [3,4] to calculate the scattering cross section of the spherical obstacle. Figure 4(a) shows the $n = 1$ order normalized scattering cross section of a single spherical obstacle embedded in the type I DZIM (blue dotted line) as a function of the radius r_d of the sphere (around the first resonance shown in Fig. 3); as a comparison, the normalized scattering cross section of the same spherical obstacle embedded in the background medium Si (red solid line) is also presented. It can be seen in the inset of Fig. 4(a) for the zoom-in view that the normalized scattering cross section of the spherical obstacle in the background medium is much larger than that of the spherical obstacle in the type I DZIM when the obstacle is off resonance. This is because of the wavelength in the type I DZIM is 10^3 times larger than that in the background medium; thus, the wave cannot "see" the obstacle. However, when the obstacle is on resonance, the normalized scattering cross section of the obstacle is drastically enhanced by orders of magnitude in the type I DZIM. As a result, we may expect that even a single sphere can be used to achieve the total blocking of a very large type I DZIM region. Note that the displacement field in the type I DZIM region disappears when the total blocking occurs; thus, the multiple scattering among the spheres does not need to be considered, and the total blocking condition ($E_{11}E_{22} - E_{12}E_{21} = 0$) is unrelated to the structure period;

a is reasonable. In addition, the normalized scattering cross sections of the spherical obstacle in the type I DZIM for $n = 0$ and $n = 2$ order are also calculated, respectively, and shown in Fig. 4(b). As can be seen, the normalized scattering cross sections for $n = 0$ and $n = 2$ order are $10^{15}-10^{16}$ orders of magnitude less than that of $n = 1$ order. Therefore, the rationality of our analytic model considering $n = 1$ order scattering only is validated.

B. Case of the type II DZIM

Having investigated the type I DZIM, we now consider the transmission property of another type of DZIM. Possessing near zero reciprocal of bulk modulus $1/\kappa$, near zero mass density ρ and ordinary shear modulus μ, type II DZIM has double near zero parameters only for the P wave, while single near zero parameter for the S wave. In contrast to type I DZIM, type II DZIM exhibits a very different propagation property because the bulk modulus instead of shear modulus diverges. Although, the purely P wave with uniform displacement field u_{1x} can still propagate in the homogeneous type II DZIM [Eq. (5)], coupled P and S waves will take the place of the purely P wave if obstacles are introduced. We can understand this difference using the constitutive relation of solid [Eq. (2)]. In the type II DZIM region, under the condition κ_1 diverges, Eq. (2) can be simplified to

$$0 = \frac{\partial v_x}{\partial x} + \frac{\partial v_y}{\partial y} + \frac{\partial v_z}{\partial z}, \quad \frac{\partial \tau_{xy}}{\partial t} = \mu\left(\frac{\partial v_x}{\partial y} + \frac{\partial v_y}{\partial x}\right),$$
$$\frac{\partial \tau_{xz}}{\partial t} = \mu\left(\frac{\partial v_x}{\partial z} + \frac{\partial v_z}{\partial x}\right), \quad \frac{\partial \tau_{yz}}{\partial t} = \mu\left(\frac{\partial v_y}{\partial z} + \frac{\partial v_z}{\partial y}\right). \tag{7}$$

Obviously, solutions $v_{1x} = \text{constant}$, $v_{1y} = v_{1z} = 0$ (for the purely P wave) cannot satisfy Eq. (7); thus, coupled P and S waves need to be considered when elastic discontinuities appear.

Figure 5(a) shows the numerically calculated transmission coefficients as a function of the radius r_d of spherical steel obstacle. In the simulation, we have set $\rho_1 = 0.001\rho_0$, $\mu_1 = \mu_0$, and $1/\kappa_1 = 0.001(1/\kappa_0)$ for the type II DZIM. The transmission spectrum is featured by several Fano-like dip. The Fano resonance is created by the interference between two different transmission channels: One is the direct transmission process that provides a continuum spectrum as background, and the other is associated with the discrete resonant state that finally leads to an asymmetric line shape featured by a couple of dips or peaks in the spectrum. In general, the Fano-like spectrum could stem from two different mechanisms: the local resonant modes in individual structural units and the collective lattice resonance effect. In the current case, the collective lattice resonance, i.e., the Wood's anomaly occurring at the wavelength near the structural period, obviously has no effect on the transmission, as the wavelength of wave in the type II DZIM is much larger than the structural period. Therefore, the local resonant modes should be responsible for the Fano-like dips. Any resonance associated with a single sphere should be reflected in the Mie scattering coefficients, such as T_n^{ll} (for P wave to P wave scattering), with n being an integer that denotes the order of the channel for spherical scattering waves. Figure 5(b) shows the $|T_n^{ll}|$ as a function of the radius r_d of

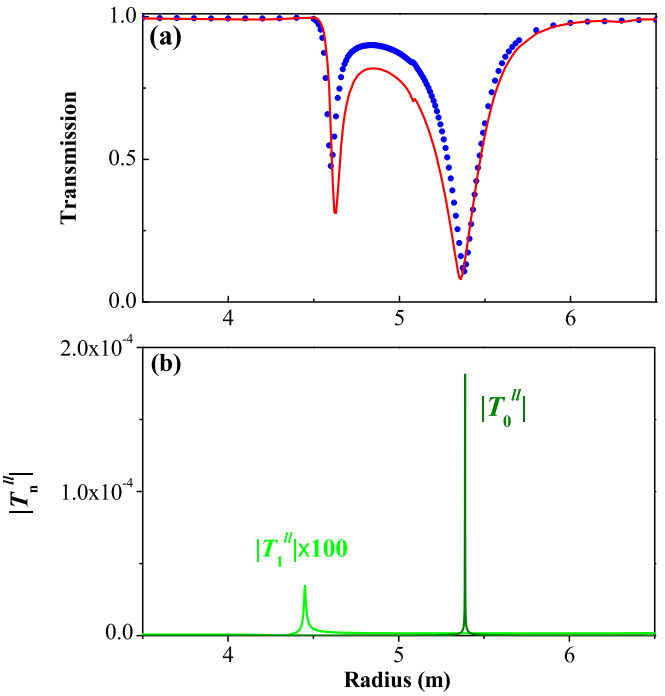

FIG. 5. The numerically calculated transmission coefficients (a) of the type II DZIM slab with spherical obstacles and the Mie scattering coefficients $|T_n^{ll}|$ (b) of the spherical obstacle in the type II DZIM as a function of the radius r_d of the spherical obstacle, respectively. In (a), the red solid and blue dotted lines represent the systems with different structure periods $a = 30$ m and $a = 36$ m, respectively.

the sphere for the lowest two orders ($n = 0, 1$). The spectra for $|T_0^{ll}|$ and $|T_1^{ll}|$, respectively, display pronounced sharp peaks, revealing characters of local modes. Compared with Fig. 5(a), we can see that the local resonant modes of single sphere result in the Fano-like dips indeed. In fact, we note that there has been a simple analytic model [42,43], which can explain the line shapes of the observed transmission resonances. In addition, it should be noted that when we increase the structure period $a =$ 30m to $a = 36$m, the transmission dips in Fig. 5(a) become shallower and move closer to the radii where local resonances arise, which is totally different to the case of the type I DZIM. The origin of this difference comes from the fact that the displacement field in the type I DZIM region disappears when the total blocking occurs; thus, the coupling of the resonant modes between neighboring spheres does not need to be considered; for the type II DZIM, there is coupling of the resonant modes obviously. This implies that the displacement field still exists in the type II DZIM region when the resonances occur.

To further distinguish the different propagation characteristics of the two types of DZIM, Fig. 6 show the numerically calculated displacement field distributions of P wave transmitting through the type II DZIM slab without/with steel spheres, respectively. Figure 6(a) shows the displacement field distributions of the P wave transmitting through the type II DZIM slab without inclusion, and the displacement field u_{1x} in the type II DZIM region is uniform indeed. Figure 6(b) shows the displacement field distributions of the P wave transmitting through the type II DZIM slab embedded with steel spheres

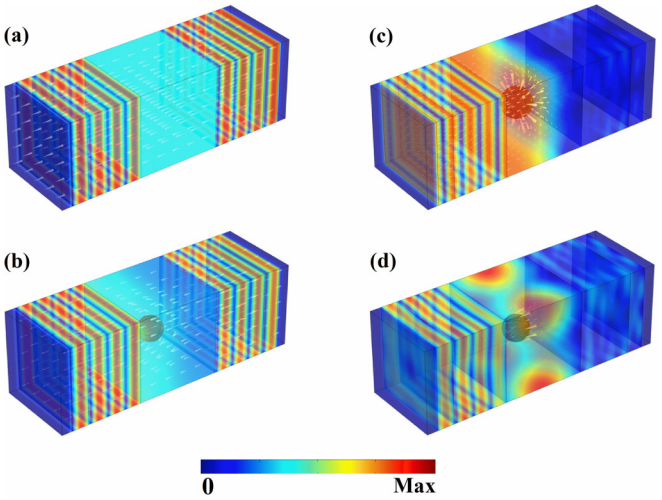

FIG. 6. The numerically simulated displacement field distributions of the incident P wave transmitting through the type II DZIM slab without inclusion (a), with spherical steel inclusions being off resonance (b), with the inclusions having monopole resonance (c), and with the inclusions having dipole resonance (d). The white arrows denote the directions of the displacement.

($r_d = 4.5$ m), which is away from the resonant radii. It can be seen that the displacement field is no longer uniform, and u_{1x}, u_{1y}, and u_{1z} appear (indicated by the arrow) in the type II DZIM region. However, the wavelength of the P wave in type II DZIM is very large, no resonant mode has arisen at this radius, and the scattering is so weak that the incident P wave can transmit through the slab with little disturbance and preserve its P wave form. In Figs. 6(c) and 6(d), we consider the embedded spheres associated with the $n = 0$ and $n = 1$ orders local resonant mode. In contrast to Fig. 2 (g), the displacement field inside the type II DZIM region does not disappear and strong monopole and dipole resonant modes concentrate in the spheres. Note that as the displacement field is no longer constant in the type II DZIM region, there is no restriction that the angular quantum number n of the displacement fields inside the spheres must take one. Thus, the analytic model, which explains the essence of the physics of total reflection in the type I DZIM, can no longer be used here.

C. Case of the SZIM

To fully understand propagation feature of various kinds of elastic ZIM, we study SZIM in this section. It is found that various types of SZIM have similar propagation properties; thus, only the result of the SZIM with near zero mass density is presented as an example. We start with calculating the transmission coefficient of the SZIM slab without embedded obstacles. Because the geometry is very simple, the calculation is pretty straightforward:

$$T = \frac{1}{1 - ik_{0l}\frac{l}{2}}, \tag{8}$$

for the incident P wave and

$$T = \frac{1}{1 - ik_{0t}\frac{l}{2}}, \tag{9}$$

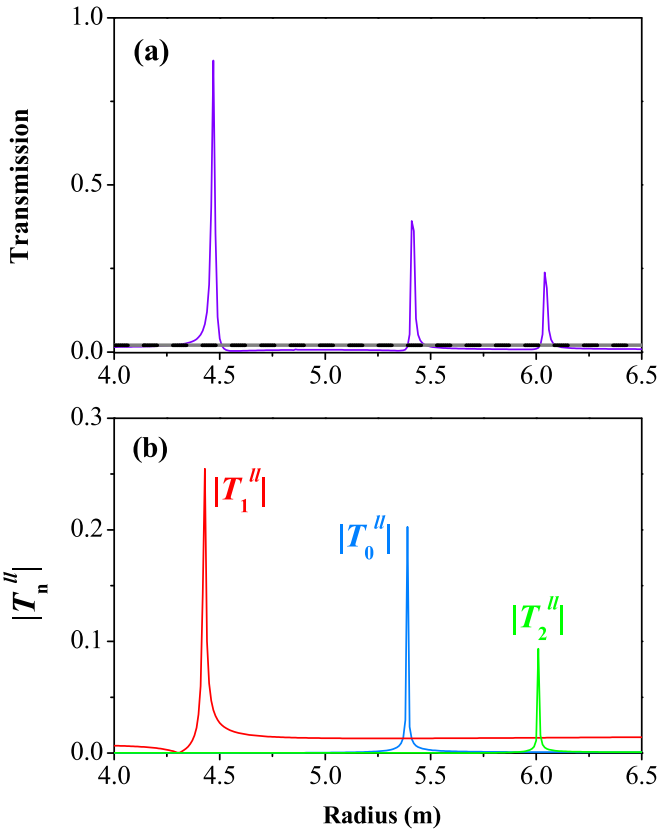

FIG. 7. The numerically calculated transmission coefficients (a) of the SZIM slab with spherical obstacles and the Mie scattering coefficients $|T_n|$ (b) of the spherical obstacle in the SZIM as a function of the radius r_d of the spherical obstacle, respectively.

for the incident S wave. In addition, k_{0l} and k_{0t} are the wave vector of P and S waves in the background medium, respectively. Equations (8) and (9) imply that only part of the incident wave can transmit through the SZIM slab because of the impedance mismatch and the transmission is inversely proportional to the width of slab.

The transmission changes if inclusions are embedded into the SZIM slab. We note that utilizing the condition $\rho_1 = 0$ cannot simplify Eqs. (1) and (2), so it would be very difficult to obtain the transmission coefficient analytically. In Fig. 7(a), we plot the numerically calculated transmission coefficients as a function of the radius r_d of spherical steel obstacle for the incident P wave as an example. The transmission coefficients for the SZIM slab in the absence of obstacles are also plotted [the black dashed line represents the numerically calculated result, while the grey solid line represents the calculated result using Eq. (8)]. One can see that several asymmetric Fano-like peaks appear in the transmission spectra after the spheres have been introduced. Again, the collective lattice resonance does not affect the transmission, as the wavelength of wave in SZIM is also much larger than the structural period. So, the local resonant modes in a single sphere should be responsible for the Fano-like peaks. Figure 7(b) shows the $|T_n^{II}|$ as a function of the radius r_d of the obstacle for the lowest several orders ($n = 0$ to $n = 2$). The spectra display several pronounced sharp peaks, revealing characters of local

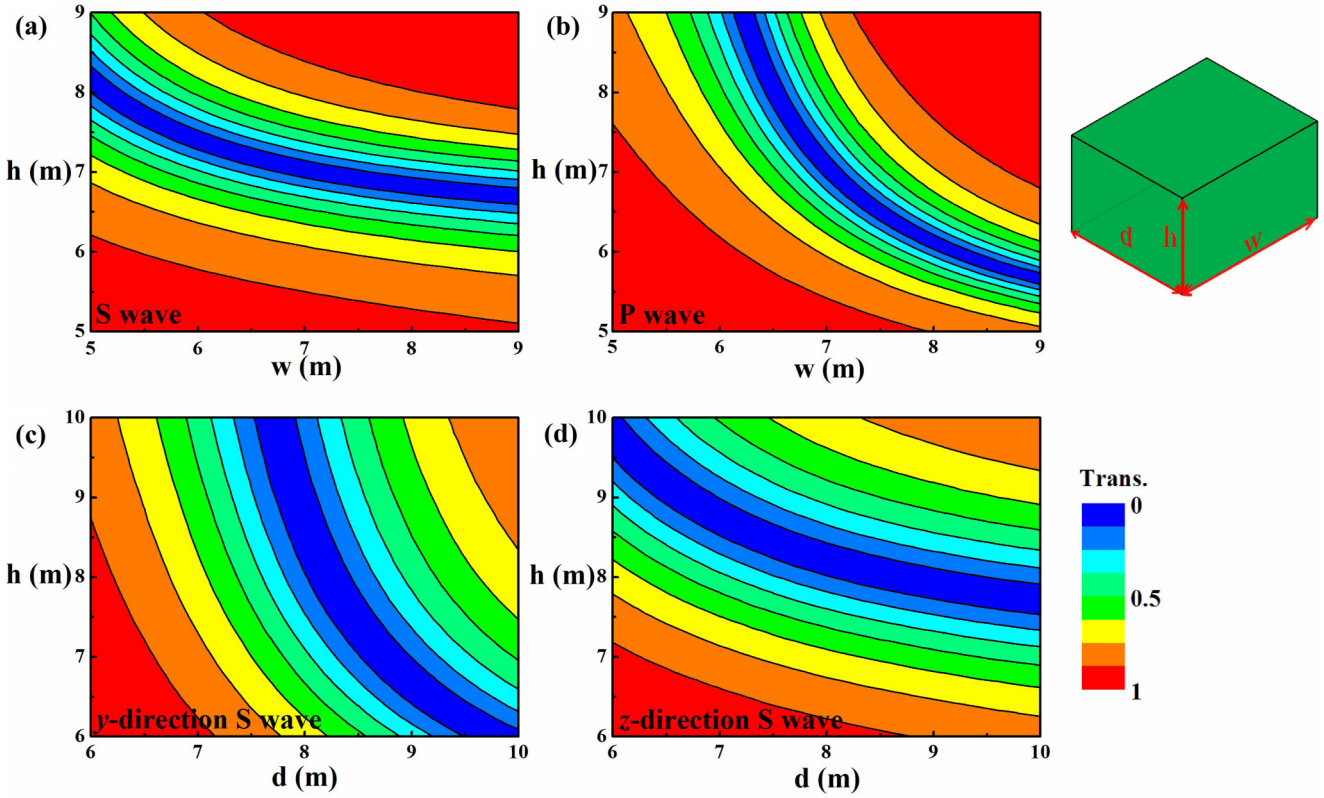

FIG. 8. The numerically calculated transmission coefficients of the type I DZIM slab with cuboid obstacles as a function of the width w and height h of the obstacle for incident S wave (a) and P wave (b), respectively. The numerically calculated transmission coefficients of the type I DZIM slab with cuboid obstacles as a function of the deep d and height h of the obstacle for incident y direction S wave (c) and z direction S wave (d), respectively. Top row represents the results of the cuboid obstacles having equal d and h. Bottom row represents the results of the cuboid obstacles having fixed $w = 5$ m.

modes. Compared with Figs. 7(a) and 7(b), we can find that the local resonant modes of single sphere result in the Fano-like peaks indeed.

III. INDEPENDENT MANIPULATION OF THE PROPAGATION OF THE *P* WAVE AND TWO *S* WAVES BY USING CUBOID OBSTACLES

Since mode conversion does not happen and the wave natures of the P wave and two S waves always remain intact during the scattering process in the type I DZIM, we investigate the possibility of independent control the propagation of P wave and two degenerate S waves by using complicated inclusions. The fact that the P wave and two S waves are controlled by the same factor is due to the high symmetry of the spherical obstacle. Thus, if we use obstacles with lower symmetry, to replace the spherical obstacle, the P wave and two S waves can be controlled by different factors, and independent control of P wave and two S waves can be realized. We perform the simulations for the incident P wave and two S waves into a type I DZIM slab with embedded cuboid obstacles. The transmission coefficients as a function of the varying geometric parameters (deep d, width w, and height h) of the cuboid obstacle are calculated for the P wave and two S waves, respectively. In the first case, we would like to independently control P waves and the S wave, and the steel cuboid with equal d and h is imbedded. Figures 8(a) and 8(b) show, respectively, the results for the two degenerate S waves and for the P wave, where the x axis is w and the y axis is h, and the color stands for transmission, with red for high and blue for low. As can be seen clearly, in a wide range (from 5 to 9 m) of h and w, this device has remarkably different outputs for the incidence of the two degenerate S waves and for the incidence of the P waves. In the second case, we would like to independently control the two originally degenerate S waves, and the steel cuboid with fixed $w = 5$ m is imbedded this time. Figures 8(c) and 8(d) show, respectively, the results for the y direction S wave and for the z direction S wave, where the x axis is d and the y axis is h. It can be seen clearly that in a wide range (from 6 to 10 m) of d and h, this device also has remarkably different outputs for the incidence of the y direction S wave and for the incidence of z direction S wave. Therefore, completely independent control of the P and two S waves can be achieved by using the cuboid obstacles indeed.

IV. A 3D PHONONIC CRYSTAL CAN BE MAPPED TO AN ELASTIC MATERIAL WITH EFFECTIVE ZERO ρ_{eff} AND ZERO $1/\mu_{\text{eff}}$

Finally, we investigate the experimental feasibility of the theoretical proposal. In Ref. [44], Chan *et al.* shown that a simple cubic photonic crystal exhibits a 3D Dirac-like point at the center of the Brillouin zone at a finite frequency. Using effective medium theory, the structure can be mapped to an

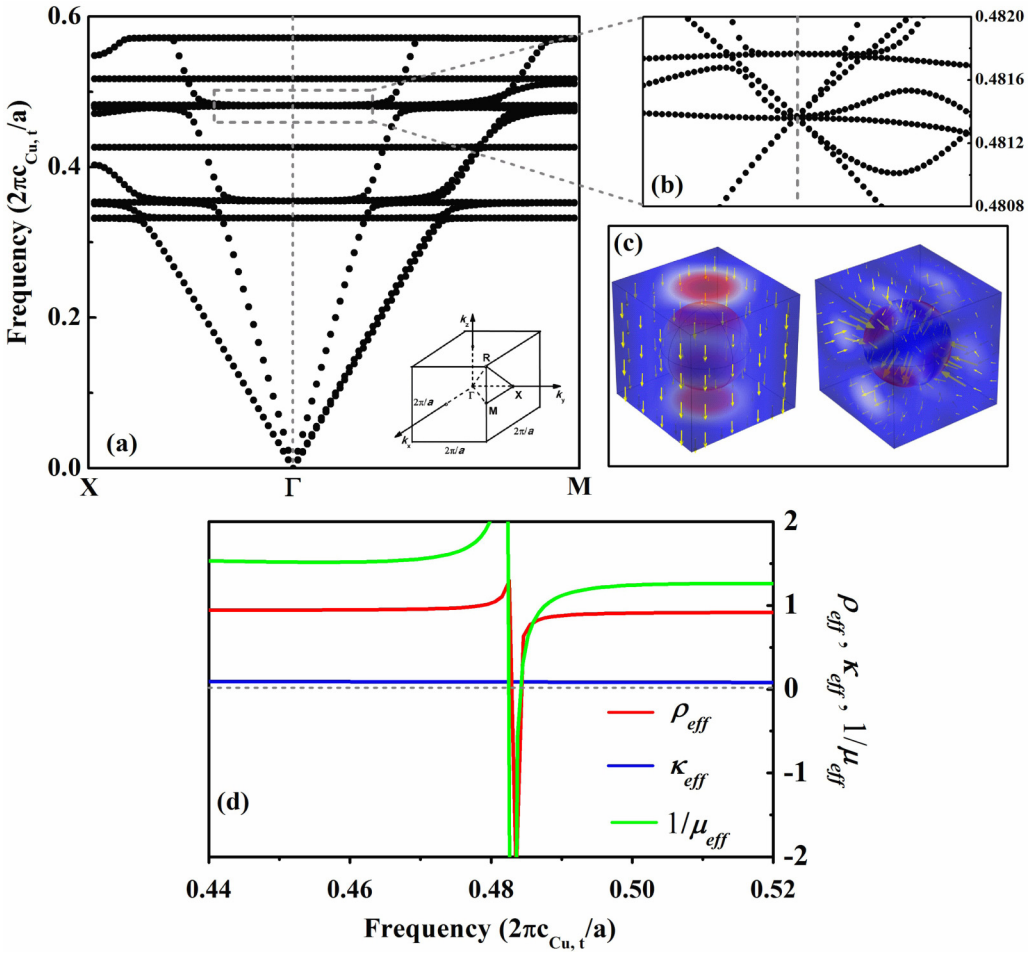

FIG. 9. (a) Band structure of a 3D simple cubic lattice phononic crystal consisting of rubber spheres embedded in Cu host. (b) The enlarged view of the band dispersion near the sixfold degenerate point frequency. (c) The displacement field distributions of the eigenstates near the sixfold degenerate point. The eigenstates are combinations of triply degenerate dipole and triply degenerate quadrupole excitations. (d) The effective mass density ρ_{eff}, bulk modulus κ_{eff}, and reciprocal of shear modulus $1/\mu_{\text{eff}}$ as a function of frequency near the sixfold degenerate point. All the effective elastic parameters have been normalized to the elastic parameters of Cu. The quantity $c_{\text{Cu},t}$ is the velocity of transverse wave of Cu. The lattice constant is denoted by a.

isotropic zero refractive index material in which the effective permittivity and permeability are simultaneously zero at the Dirac-like point frequency. The Dirac-like point is sixfold degenerate and is formed by the accidental degeneracy of electric dipole and magnetic dipole excitations, each with three degrees of freedom. In this paper, we would like to design a 3D phononic crystal system that also has Dirac-like point at the center of the Brillouin zone and can be mapped to an elastic material with effective mass density and reciprocal of shear modulus equal to zero at the Dirac-like point frequency.

Figure 9(a) shows the numerically calculated band structure of the 3D simple cubic lattice phononic crystal consisting of rubber ($\rho_{\text{rubber}} = 1.3 \times 10^3$ kg/m^3, $c_{\text{rubber},l} = 0.817 \times 10^3$ m/s, and $c_{\text{rubber},t} = 0.335 \times 10^3$ m/s) spheres embedded in the Cu ($\rho_{\text{Cu}} = 8.96 \times 10^3$ kg/m^3, $c_{\text{Cu},l} = 4.726 \times 10^3$ m/s, and $c_{\text{Cu},t} = 2.1 \times 10^3$ m/s) host. Figure 9(b) provides an enlarged view of the band dispersion in the frequency range of interest. There are two triply degenerate states at the Γ point, and they correspond to dipole modes and quadrupole modes, respectively. Through tuning the radius of the spheres, we can make the dipole modes and quadrupole modes touch each other at the same frequency. At the radius of the sphere $R = 0.343a$, with a being the lattice constant, the accidental degeneracy occurs at the frequency $\omega = 0.481(2\pi c_{\text{Cu},t}/a)$. As the dipole modes and quadrupole modes are each threefold degenerate at the zone center, the accidental degeneracy gives rise to a sixfold degenerate state at the Γ point. Four bands have linear dispersions near the Γ point, the other two bands are relatively flat. To understand the physical nature of the eigenstates near the sixfold degenerate point, we calculate the displacement field distributions of the eigenstates at the Dirac-like point frequency. Figure 9(c) demonstrates the dipole and the quadrupole excitations along the z direction. The arrows show the directions of the displacement field. The eigenstates of the other four modes at the Dirac-like point frequency correspond to dipole and quadrupole excitations along x and y directions (not shown here). Therefore, the 3D accidental degeneracy-induced Dirac point can be described by dipole and quadrupole excitations along the x, y, and z directions.

We have shown previously that in a two-dimensional (2D) phononic crystal, the Dirac-like point that is derived from the

accidental degeneracy of dipole and quadrupole excitations can be mapped to a zero-refractive-index at that frequency [39]. Is it possible to describe the Dirac-like point physics of the 3D phononic crystal system with effective medium theory? We apply the effective medium theory [45] to calculate the effective medium of this 3D system. The results are plotted in Fig. 9(d), in which the red, blue, and green lines represent ρ_{eff}, κ_{eff}, and $1/\mu_{\text{eff}}$ as a function of frequency, respectively. Figure 9(d) clearly shows that ρ_{eff} and $1/\mu_{\text{eff}}$ intersects at zero at the sixfold degenerate point ($\omega = 0.481(2\pi c_{\text{Cu},t}/a)$). Because the eigenmode is a combination of quadrupolar and dipolar states only [Fig. 9(c)], κ_{eff} does not exhibit resonant behaviors in the frequency region considered. As ρ_{eff} and $1/\mu_{\text{eff}}$ go through zero simultaneously and linearly, the effective refractive index also goes through zero but the group velocity remains finite. Consequently, we realize type I DZIM in the 3D phononic crystal system. We consider that type II DZIM and various types of SZIM can be realized by using 3D phononic crystal in a similar way.

V. CONCLUSIONS

In conclusion, the scattering properties of elastic waves by 3D obstacles in various types of elastic ZIM have been theoretically investigated. In the type I DZIM, mode conversion does not occur and the wave natures remain intact during the scattering process; while in the type II DZIM mode conversion occurs, and many other transmission features are also different to the former. For SZIM, only part of the incident wave can transmit through the SZIM slab without inclusions, but the transmission can be strongly enhanced by introducing obstacles with resonant modes. Moreover, utilizing the propagation characteristics of the type I DZIM, we realize completely independent control the propagation of P wave and S waves (even the two S waves are originally degenerate) by introducing obstacles with low symmetry. A 3D phononic crystal system is suggested to achieve the intriguing phenomena. Our results provide full understanding of scattering of elastic waves by 3D obstacles in metamaterials with zero index and thus enable a way of controlling the propagation of them.

ACKNOWLEDGMENTS

This paper is supported by the National Natural Science Foundation of China (Grants No. 11674088, No. 11304090, 11504103, and No. 11404107).

APPENDIX

Let us consider using the case of the incident P wave as an example, the derivation for incident S waves is similar. Suppose a plane harmonic P wave $u_x^{\text{inc}} = u_x e^{i(k_{0l}x-\omega t)}$ is incident from left into the unit cell presented in Fig. 1, where u_x is the amplitude of the incident field, k_{0l} is the wave vector in the background medium, and ω is the angular frequency. We omit the time variation item in the rest of this section for convenience. Thus, the displacement field in the left background region can be written as

$$u_{0x} = u_x\left[e^{ik_{0l}x} + \text{Re}^{-ik_{0l}x}\right], \tag{A1}$$

while in the right background region, the displacement field must have the form

$$u_{2x} = u_x T e^{ik_{0l}(x-l)}, \tag{A2}$$

where R and T are the reflection and transmission coefficients. In the type I DZIM region, the displacement field maintains a quasistatic situation ($u_{1x} =$ constant, regardless of whether there are obstacles). Then, using the continuous boundary condition at $x = l$, we have $u_x T = u_{1x}$; thus, $T = u_{1x}/u_x$. Obviously, $T = 0$ (total blocking) occurs if $u_{1x} = 0$, which means that the displacement field disappears anywhere in the type I DZIM region. In fact, it can be seen from Fig. 2(g) that the displacement field u_{1x} inside the type I DZIM region disappears indeed. Then, we need to find out how to obtain $u_{1x} = 0$. In the embedded solid spheres, the displacement field $\mathbf{u_d}$ is described by the elastic wave equation

$$(\lambda_d + 2\mu_d)\nabla(\nabla \cdot \mathbf{u_d}) - \mu_d \nabla \times \nabla \times \mathbf{u_d} + \rho_d \omega^2 \mathbf{u_d} = 0, \tag{A3}$$

where λ_d represents the Lame constant. The azimuthal symmetry of the sphere implies that the displacement field in the solid sphere may be expressed in terms of potential functions as

$$\mathbf{u_d} = \nabla\phi + \nabla \times \left(\frac{\partial\psi}{\partial\theta}\vec{e}_\varphi\right). \tag{A4}$$

The solutions for ϕ and ψ may be written, respectively, as

$$\phi = \sum_{n=0}^{\infty} A_{n1} j_n(k_{dl}r) P_n(\cos\theta), \tag{A5}$$

$$\psi = \sum_{n=0}^{\infty} A_{n2} j_n(k_{dt}r) P_n(\cos\theta), \tag{A6}$$

where $k_{dl} = \omega\sqrt{\rho_d/(\kappa_d + \mu_d)}$ and $k_{dt} = \omega\sqrt{\rho_d/\mu_d}$, $j_n(x)$ are the n th-order spherical Bessel function and $P_n(x)$ is the n th-order Legendre polynomial. The displacement continuity across the sphere boundary requires that

$$u_{dr}|_{r=r_d} = u_{1x}\cos\theta, \quad u_{d\theta}|_{r=r_d} = -u_{1x}\sin\theta, \tag{A7}$$

which means that in Eqs. (A5) and (A6), we have to keep only the terms with $n = 1$ to produce the necessary θ dependence. This leads to a set of linear equations

$$E_{11}A_{11} + E_{12}A_{12} = r_d u_{1x}, \quad E_{21}A_{11} + E_{22}A_{12} = r_d u_{1x}, \tag{A8}$$

where E_{ij} is defined as $E_{11} = j_1(k_{dl}r_d) - k_{dl}r_d j_2(k_{dl}r_d)$, $E_{12} = -2j_1(k_{dt}r_d)$, $E_{21} = j_1(k_{dl}r_d)$, and $E_{22} = -2j_1(k_{dt}r_d) + k_{dt}r_d j_2(k_{dt}r_d)$. Solving Eq. (A8), we obtain

$$u_{1x} = \frac{E_{11}E_{22} - E_{12}E_{21}}{(E_{22} - E_{12})r_d}A_{11} = \frac{E_{11}E_{22} - E_{12}E_{21}}{(E_{11} - E_{21})r_d}A_{12}. \tag{A9}$$

From Eq. (A9), we can see that if $E_{11}E_{22} - E_{12}E_{21} = 0$, then $u_{1x} = 0$; thus, $T = 0$, in which case the total blocking happens. For the incident y direction or z direction S waves, after a similar processing, we find the same condition ($E_{11}E_{22} - E_{12}E_{21} = 0$) needs to be satisfied to obtain $T = 0$.

[1] C. F. Ying and R. Truell, J. Appl. Phys. **27**, 1086 (1956).
[2] N. Einspruch, E. J. Witterholt, and R. Truell, J. Appl. Phys. **31**, 806 (1960).
[3] Y. H. Pao and C. C. Mow, J. Appl. Phys. **34**, 493 (1963).
[4] G. Johnson and R. Truell, J. Appl. Phys. **36**, 3466 (1965).
[5] P. C. Waterman, J. Acous. Soc. Am. **60**, 567 (1976).
[6] G. C. Gaunaurd and H. Überall, J. Acous. Soc. Am. **63**, 1699 (1978).
[7] G. C. Gaunaurd, Appl. Mech. Rev **42**, 143 (1989).
[8] X. Zhou and G. Hu, Phys. Rev. E **75**, 046606 (2007).
[9] Z. Liu, X. Zhang, Y. Mao, Y. Y. Zhu, Z. Yang, C. T. Chan, and P. Sheng, Science **289**, 1734 (2000).
[10] G.W. Milton, M. Briane, and J. R. Willis, New J. Phys. **8**, 248 (2006).
[11] Y. Lai, Y. Wu, P. Sheng, and Z. Q. Zhang, Nat. Mater. **10**, 620 (2011).
[12] Y. Wu, Y. Lai, and Z. Q. Zhang, Phys. Rev. Lett. **107**, 105506 (2011).
[13] N. Stenger, M. Wilhelm, and M. Wegener, Phys. Rev. Lett. **108**, 014301 (2012).
[14] S. Enoch, G. Tayeb, P. Sabouroux, N. Guerin, and P. Vincent, Phys. Rev. Lett. **89**, 213902 (2002).
[15] R.W. Ziolkowski, Phys. Rev. E **70**, 046608 (2004).
[16] M. G. Silveirinha and N. Engheta, Phys. Rev. Lett. **97**, 157403 (2006).
[17] B. Edwards, A. Alù, M. E. Young, M. Silveirinha, and N. Engheta, Phys. Rev. Lett. **100**, 033903 (2008).
[18] J. Hao, W. Yan, and M. Qiu, Appl. Phys. Lett. **96**, 101109 (2010).
[19] V. C. Nguyen, L. Chen, and K. Halterman, Phys. Rev. Lett. **105**, 233908 (2010).
[20] J. Luo, W. X. Lu, Z. H. Hang, H. Y. Chen, B. Hou, Y. Lai, and C. T. Chan, Phys. Rev. Lett. **112**, 073903 (2014).
[21] X. Huang, Y. Lai, Z. H. Hang, H. Zheng, and C. T. Chan, Nat. Mater. **10**, 582 (2011).
[22] J. W. Dong, M. L. Chang, X. Q. Huang, Z. H. Hang, Z. C. Zhong, W. J. Chen, Z. Y. Huang, and C. T. Chan, Phys. Rev. Lett. **114**, 163901 (2015).
[23] Y. Li, S. Kita, P. Muñoz, O. Reshef, D. I. Vulis, M. Yin, M. Lončar, and E. Mazur, Nat. Photonics **9**, 738 (2015).
[24] C. Argyropoulos, P.-Y. Chen, G. D'Aguanno, N. Engheta, and A. Alù, Phys. Rev. B **85**, 045129 (2012).
[25] L. Caspani, R. P. M. Kaipurath, M. Clerici, M. Ferrera, T. Roger, J. Kim, N. Kinsey, M. Pietrzyk, A. Di Falco, V. M. Shalaev, A. Boltasseva, and D. Faccio. Phys. Rev. Lett. **116**, 233901 (2016).
[26] F. Bongard, H. Lissek, and J. R. Mosig, Phys. Rev. B **82**, 094306 (2010).
[27] Z. Liang and J. Li, Phys. Rev. Lett. **108**, 114301 (2012).
[28] F. M. Liu, X. Q. Huang, and C. T. Chan, Appl. Phys. Lett. **100**, 071911 (2012).
[29] J. Mei, Y. Wu, C. T. Chan, and Z. Q. Zhang, Phys. Rev. B **86**, 035141 (2012).
[30] D. Torrent and J. Sanchez-Dehesa, Phys. Rev. Lett. **108**, 174301 (2012).
[31] J. J. Park, K. J. B. Lee, O. B. Wright, M. K. Jung, and S. H. Lee, Phys. Rev. Lett. **110**, 244302 (2013).
[32] Y. Xie, B.-I. Popa, L. Zigoneanu, and S. A. Cummer, Phys. Rev. Lett. **110**, 175501 (2013).
[33] R. Fleury and A. Alu, Phys. Rev. Lett. **111**, 055501 (2013).
[34] Q. Wei, Y. Cheng, and X. J. Liu, Appl. Phys. Lett. **102**, 174104 (2013).
[35] L. Y. Zheng, Y. Wu, X. Ni, Z.-G. Chen, M.-H. Lu, and Y.-F. Chen, Appl. Phys. Lett. **104**, 161904 (2014).
[36] S. Y. Yu, Q. Wang, L. Y. Zheng, C. He, X. P. Liu, M. H. Lu, Y. F. Chen, Appl. Phys. Lett. **106**, 151906 (2015).
[37] F. M. Liu, Y. Lai, X. Q. Huang, and C. T. Chan, Phys. Rev. B **84**, 224113 (2011).
[38] T. Antonakakis, R. V. Craster, and S. Guenneau, New J. Phys. **15**, 103014 (2013).
[39] F. M. Liu and Z. Y. Liu, Phys. Rev. Lett. **115**, 175502 (2015).
[40] K. F. Graff, *Wave Motion in Elastic Solids* (Dover, New York, 1991).
[41] Z. Liu, C. T. Chan, and P. Sheng, Phys. Rev. B **71**, 014103 (2005).
[42] G. Gantzounis and N. Stefanou, Phys. Rev. B **72**, 075107 (2005).
[43] R. Sainidou and N. Stefanou, Phys. Rev. B **73**, 184301 (2006).
[44] C. T. Chan, X. Huang, F. Liu, and Z. H. Hang, Prog. Electromagn. Res. B **44**, 163 (2012).
[45] Y. Q. Ding, Z. Y. Liu, C. Y. Qiu, and J. Shi, Phys. Rev. Lett. **99**, 093904 (2007).